

# Mechanical anisotropy of columnar jointed basalts: An example from the Baihetan hydropower station, China



Quan Jiang<sup>a,\*</sup>, Xia-ting Feng<sup>a</sup>, Yossef H. Hatzor<sup>b</sup>, Xian-jie Hao<sup>a</sup>, Shao-jun Li<sup>a</sup>

<sup>a</sup> State Key Laboratory of Geomechanics and Geotechnical Engineering, Institute of Rock and Soil Mechanics, Chinese Academy of Sciences, Wuhan 430071, China

<sup>b</sup> Department of Geological Environmental Sciences, Ben-Gurion University of the Negev, Beer-Sheva 84105, Israel

## ARTICLE INFO

### Article history:

Received 9 November 2013

Received in revised form 18 March 2014

Accepted 31 March 2014

Available online 12 April 2014

### Keywords:

Mechanical anisotropy

Transverse isotropy

Columnar basalts

Rock joints

Rock mass

## ABSTRACT

Columnar jointed basalts are characterized by a self-organized joint network of discontinuities and pose a difficult challenge for geotechnical engineering design due to their inherent anisotropic nature. We explore here the anisotropic characteristics of the columnar basalt formation in the Chinese Baihetan hydropower station, including aspects of the geometrical rock structure, deformation, and strength anisotropy. Site investigations reveal that a typical cross section of the columnar basalt blocks is mainly quadrangular and pentagonal with an average edge length of 0.152 m. Three types of joints with different macro- and micro-characteristics form the columnar jointed rock mass and are identified by scanning electron microscopy. In situ ultrasonic tests further confirm that the columnar basalt prisms exhibit transverse isotropy with the plane of isotropy perpendicular to the column axis, as can also be observed in the field. Strength anisotropy is confirmed by point load and uniaxial compression tests. The mechanical and anisotropic characteristics of Baihetan's jointed basalt mass can be explained by its multi-scale joints pattern by means of Goodman's stiffness equation. We find that the anisotropic coefficients obtained for its deformability and strength are similar for all testing methods employed, including in situ *P* wave velocity, point load tests, and uniaxial compression tests. This result confirms the strong anisotropic effect in these rock masses and facilitates, an issue that must be considered when assigning input parameters for various classification and numerical analyses schemes.

© 2014 Elsevier B.V. All rights reserved.

## 1. Introduction

Conventional wisdom in rock mechanics states that structural joints affect the mechanical response of the rock mass by introducing strong anisotropic effects (Barton and Bandis, 1980; Hudson and Priest, 1983; Brady and Brown, 1985; Pariseau, 1999; Diego et al., 2011). If the joint sets have a reasonably uniform orientation and are closely spaced and continuous, the overall rock mass behavior may be assumed to be equally isotropic and can be modeled using empirical classification methods (Hoek and Brown, 1980; Moon et al., 2005; Gadde et al., 2007; Wang et al., 2011). This approach is based on the cumulative engineering experience of multiple workers and has been empirically validated and theoretically affirmed (Yoshida and Horii, 2004; Maghous et al., 2008; Zhang et al., 2012). Nevertheless, a discontinuous rock mass must be considered an anisotropic material if the joint sets are distributed with a few principal directions and characteristic spacing distributions (Cundall and Fairhurst, 1987; Hoek et al., 1998; Wu and Wang, 2001; Budetta and Nappi, 2011; Fortsakis et al., 2012). Due to the low shear and tensile strengths of intensely jointed rock masses, load–unload cycles may exhibit significant hysteresis, and greater deformation

may ensue along certain preferred orientations, leading to structurally controlled failure patterns (Ishida and Uchita, 2000). Under certain extreme conditions, discontinuities with adverse attitudes to the opening face may trigger great disasters during underground excavation (Gencer, 1985; Sousa, 2006; Jaeger et al., 2007; Jia and Tang, 2008).

A columnar jointed basalt rock mass, which typically originates from lava flow, is characterized by a special geological structure in which the joint network is self-organized into a roughly hexagonal arrangement and leaves behind an ordered colonnade. The widely accepted current view regarding the formation of columnar jointing involves a thermally induced contraction–cooling mechanism (Peck and Minakami, 1968; Degraff et al., 1989; Budkewitsch and Robin, 1994; Müller, 1998; Lore et al., 2000; Goehring et al., 2006). While the columnar basalt formation mechanism is fairly well understood, the geotechnical characteristics of such a rock mass are less well established. Moreover, joint-set orientation and spacing dictate the failure modes expected in any given free face around the excavated space. (Ibarra et al., 1996; Waltham and Swift, 2004; Mahendra and Bhawani, 2008; Fuenkajorn and Phueakphum, 2010).

Rock masses composed of columnar basalts exist in many places throughout China; in certain areas, they compose popular scenic spots (Zhu et al., 1985; Fang et al., 2011). As in the rest of the world, in China, most research efforts have concentrated on the columnar basalt

\* Corresponding author. Tel.: +86 27 87198805; fax: +86 27 87197610.  
E-mail address: [qjiang@whrsm.ac.cn](mailto:qjiang@whrsm.ac.cn) (Q. Jiang).

origin and formation mechanism. In recent years, certain large geotechnical hydropower and highway projects have exposed its unfavorable properties in engineering geology (Xu et al., 2010; Yan et al., 2011). Notably, the columnar jointed basaltic rock mass in the Baihetan hydropower station has exhibited serious stability issues, including sliding, fracturing, and collapse (Shi et al., 2008). Therefore, it is essential to address the geotechnical and geomechanical characteristics of such a rock mass through field and laboratory studies to minimize future failures in underground openings that are excavated in columnar basalts.

In this paper, we focus on the anisotropic nature of a columnar jointed basalt (CJB), where typically the plane of isotropy is orthogonal to the columnar rock block longitudinal axis. The special anisotropic characteristics of the CJB, including the anisotropic structure of the rock mass, three micro-scale characteristics of joint surfaces, and the deformation moduli and compressive strength anisotropies, were analyzed through field surveys, scanning electron microscopy, in situ ultrasonic tests, field point load tests, and laboratory uniaxial compressive tests. Based on this comprehensive study we present preliminary estimates for mechanical parameters of the CJB that can be used as input parameters in classification methods or numerical approaches which may be employed to predict the mechanical response of CJB during underground or surface excavations.

## 2. Geological and geotechnical settings for the Baihetan hydropower station

The planned Baihetan hydropower station will be located at the border between Ningnan County of Sichuan Province and Qiaojia County of Yunnan Province downstream of the Jinsha River (Figure 1a). The station has an electrical capacity of 16 GW and will function as a very

large multipurpose water conservancy project, similar to the Three Gorges hydraulic station. The valley region is characterized by canyon geomorphology with the general stratum inclining to the southeast (Shi et al., 2006; Xu et al., 2011). The station consists of several parts: the left underground hydraulic caverns, the right underground hydraulic caverns, the arched concrete dam, and five diversion tunnels.

The stratigraphic column belongs to the Emei mountain group of the Permian system ( $P_2\beta$ ) and is a basaltic formation originated from magmatic and volcanic eruptions. The basalt flow layers are inclined with strike trending  $N30^\circ-50^\circ E$  and a dip angle of  $SE \angle -15^\circ-25^\circ$ . The volcanic sequence can be divided into 11 rock layers ( $P_2\beta_1 \sim P_2\beta_{11}$ ) according to recognized and identified historic lava eruption episodes. The columnar jointed rock mass is fully developed among the  $P_2\beta_3$  layers (i.e. the  $P_2\beta_3^2$  and  $P_2\beta_3^3$  layers, as shown in Figure 1b). The representative rock mass in these rock layers are gray-black jointed basalt with prismatic blocks and a columnar joint network. Except for the effect from local tectonic activity, the CJB prismatic block axis has a plunge angle of approximately  $60-85^\circ$ .

During excavation of the CJB rock mass in the diversion tunnels (typically 19.7 m wide and 24.2 m high in the transverse section), special unloading failure characteristics were revealed in the following sequence of events: First, the columnar joints parallel to prismatic rock blocks began to exhibit incremental loosening and splaying following excavation, most likely induced by unloading the initially stressed rock mass; Next, transverse joints transecting the prismatic blocks began to open due to unloading over several days; Finally, prismatic rock block release and collapse into the excavation space followed if temporary support measures were not installed (Figure 2). Field investigations clearly indicated that the CJB deformation pattern and failure modes differed between the opening faces parallel and normal to the

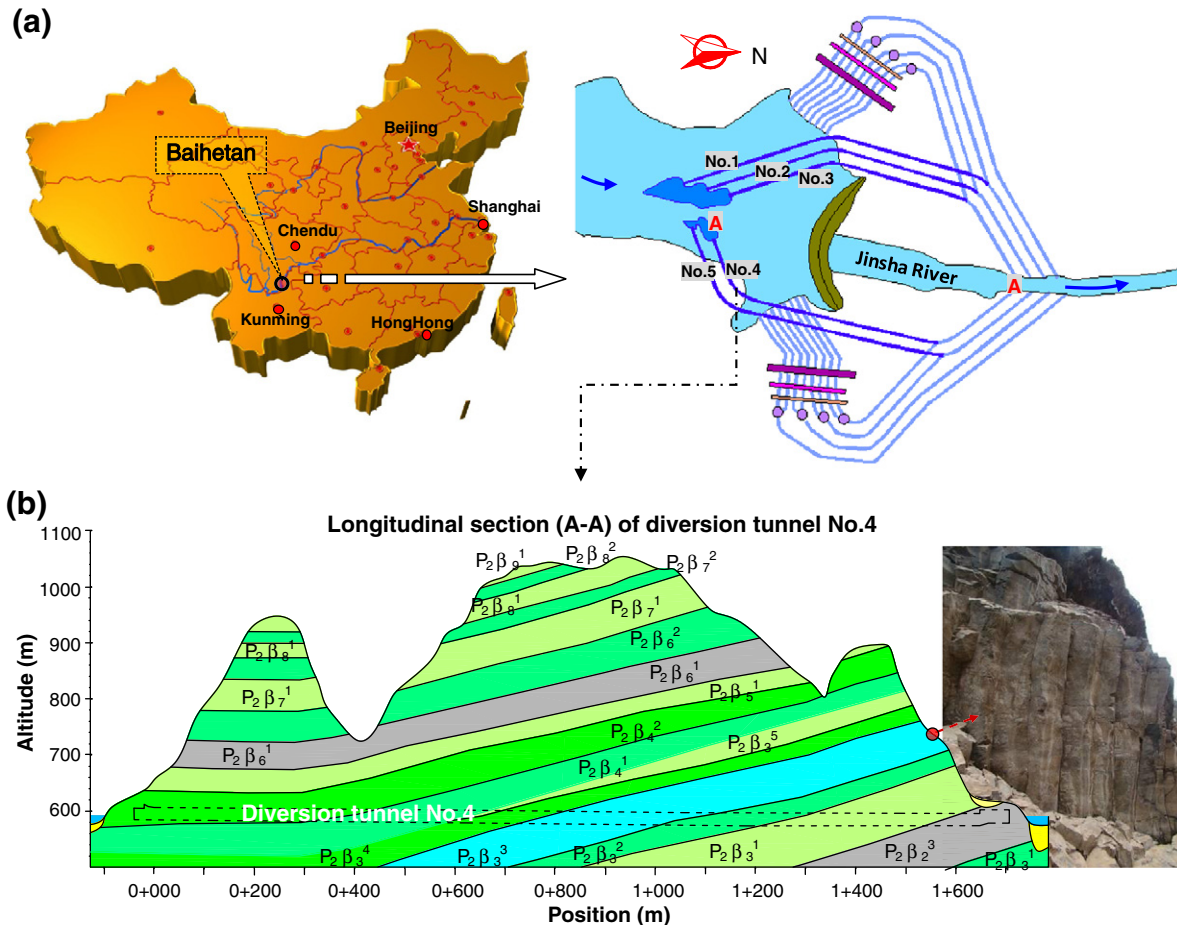


Fig. 1. The layout and geological setting of the Baihetan hydropower station: a) location map and project layout, and b) the exposed columnar jointed basalt in the No. 4 diversion tunnel.

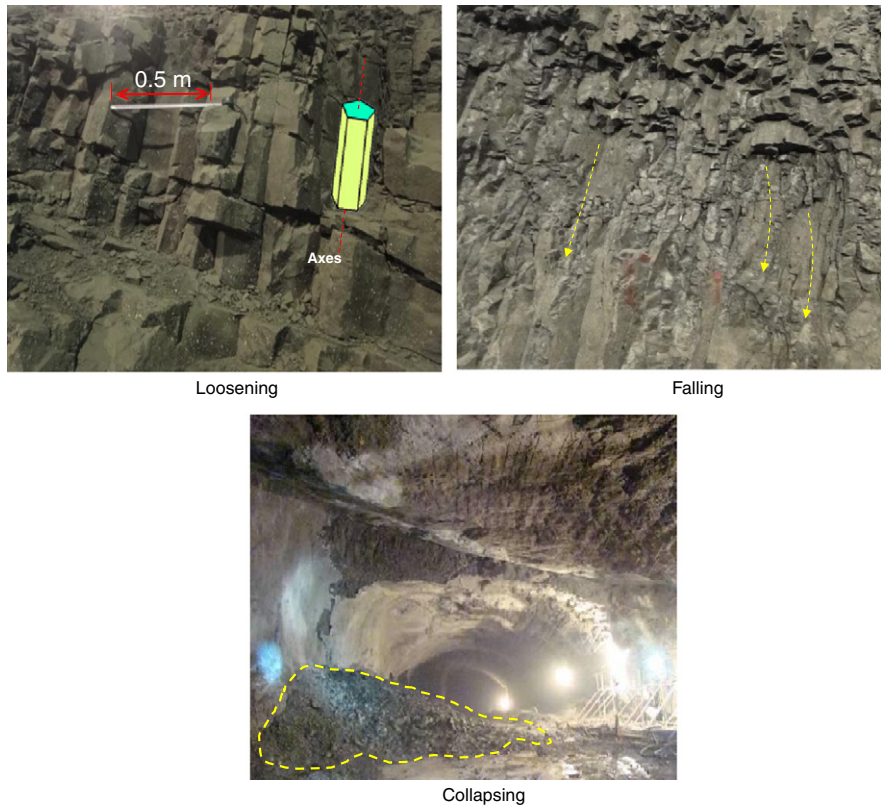


Fig. 2. Representative failure modes of the columnar jointed basalt in the Baihetan diversion tunnels.

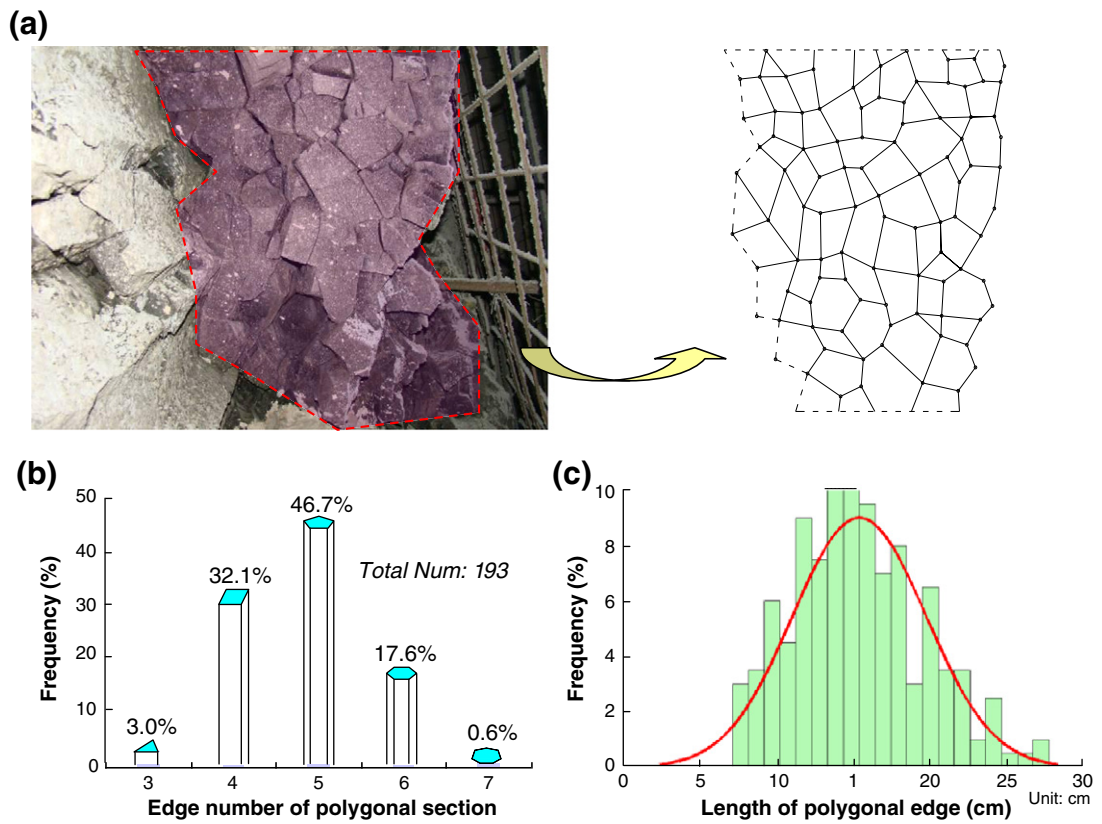


Fig. 3. Cross section (a) and statistical characteristics (b, c) of typical columnar basalt blocks.

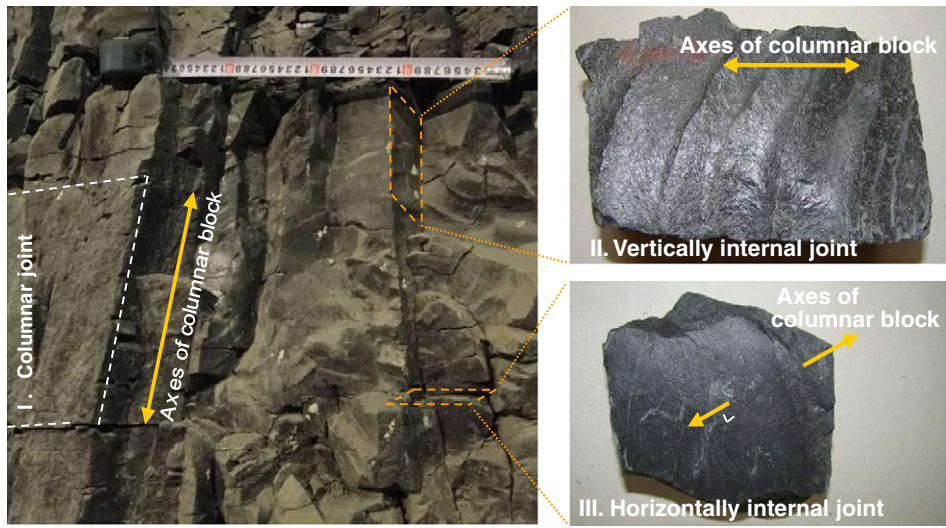


Fig. 4. Three types of joint sets and their relationship to the axes of the prismatic columnar basalt rock blocks.

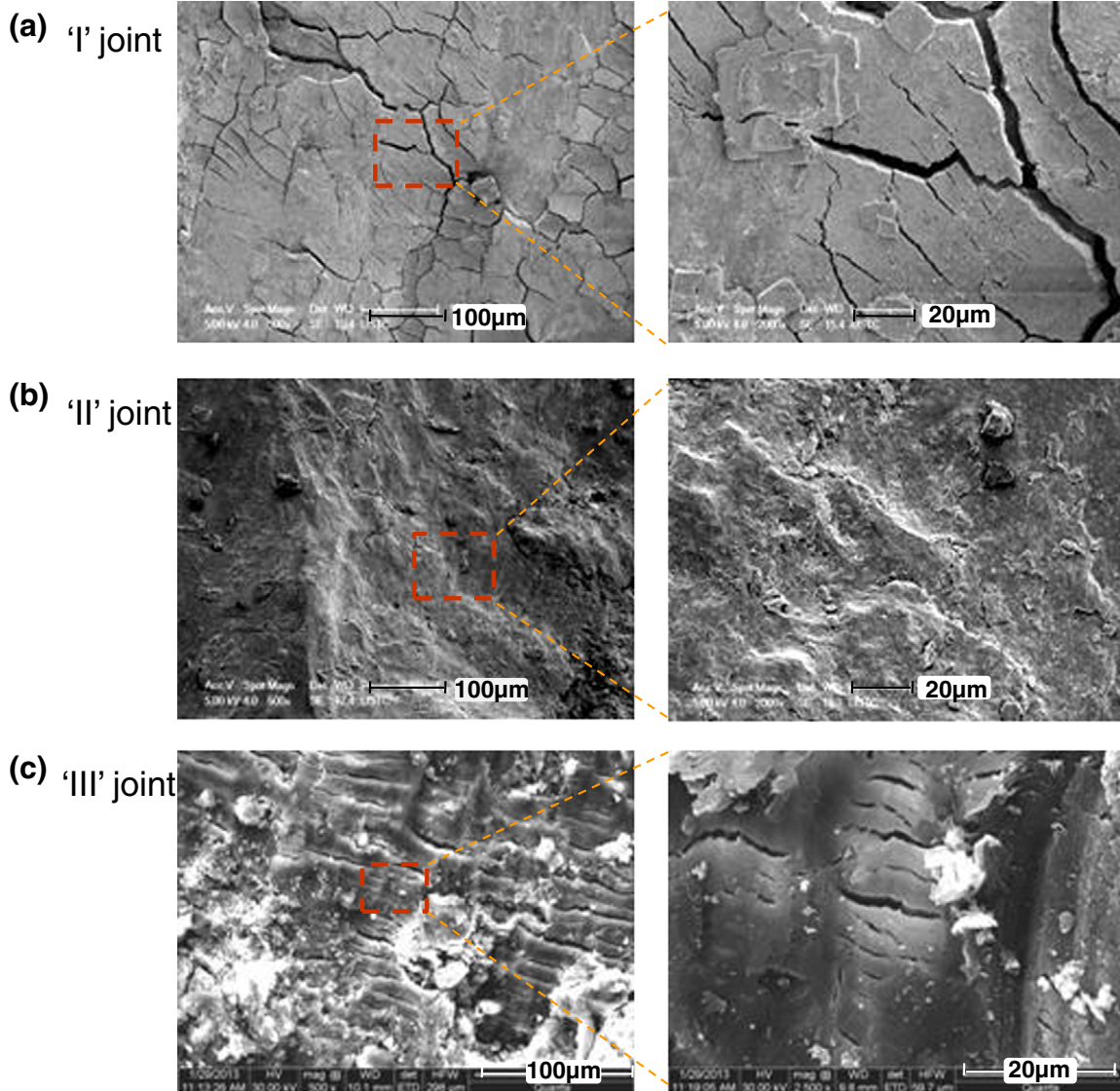


Fig. 5. SEM images of representatives for the three joint types identified in columnar basalt blocks.

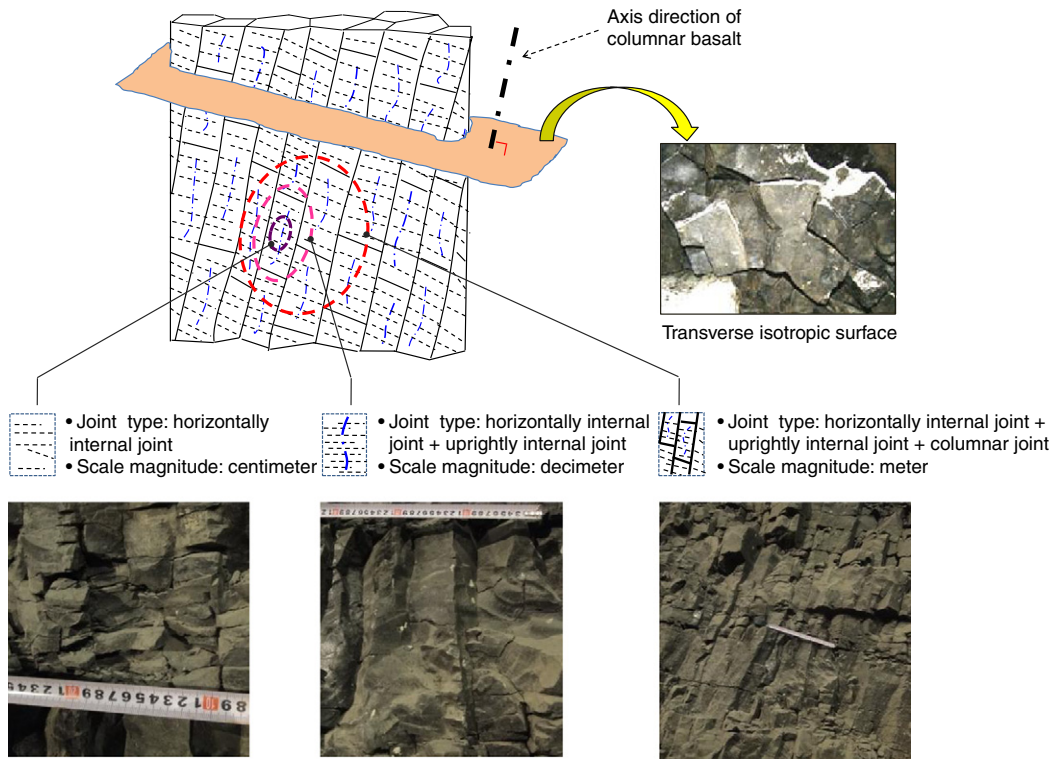


Fig. 6. The transverse isotropy plane (shaded) and multi-scale joints comprising the columnar jointed basalt (CJB) rock mass structure.

prismatic basalt block axes. Therefore, the geomechanical behavior of CJB in the diversion tunnels was highly dependent upon the anisotropic nature of the columnar basalt rock mass. Understanding the significance of inherent rock mass anisotropy, in this case due to the nature of the internal structure of the columnar basalt, is essential for the appropriate design of support for the five diversion tunnels and other subsequent underground large caverns and tunnels associated with this project, such as the underground main powerhouse and the downstream surge tank.

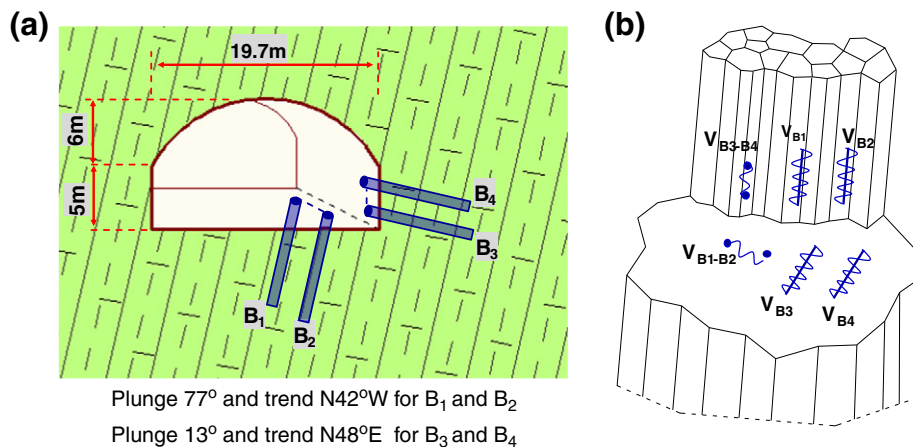
### 3. The anisotropic structure of the columnar basalts

#### 3.1. Field characteristics of the columnar basalts

Field investigations in Baihetan's diversion tunnels showed that the exposed rock mass structure in the roof and sidewalls was dominated by prismatic rock blocks formed by the assembly and intersection of

joint sets, which compose the overall rock mass structure. The typical height of the prismatic blocks ranged from several decimeters to 1 m due to the varying spaces between the transverse joints that are normal to the prismatic block axis. Interestingly, the transverse sections of a typical columnar rock block were not always hexagonal (Figure 3a). Statistical measurements of almost 200 block sections performed in the field showed that the quadrangular, pentagonal and hexagonal polygon frequency in the columnar block cross section were 32.1%, 46.7% and 17.6%, respectively, and that the combined frequency of the triangular and heptagonal polygons was less than or equal to 4% of the total shapes (Figure 3b). Statistical analyses of field data also indicated that the average polygon edge length was approximately 0.152 m, and more than 80% of the edge lengths were in the range 0.12–0.24 m (Figure 3c).

The statistical result that the polygon sections were not always hexagonal but exhibited several types of polygon shapes is consistent with Hetenyi's investigations on columnar jointed rock masses from 50 regions in Europe (Hetenyi et al., 2012). According to Goehring and



Plunge 77° and trend N42°W for B<sub>1</sub> and B<sub>2</sub>  
Plunge 13° and trend N48°E for B<sub>3</sub> and B<sub>4</sub>

Fig. 7. The arranged boreholes for the ultrasonic P wave velocity tests. (a) Layout drilled boreholes, and (b) the P-wave velocity data obtained in different transmitting directions.

Morris (2008) and Hetenyi et al. (2012), the hexagonal cross section may evolve due to thermal shrinkage stress that acts on the lava surface, provided that the environmental temperature is slightly lower than the solidification temperature of the lava flow material. Otherwise, an excessively high or low temperature difference would induce disorganized extension of new or preexisting fractures during the lava cooling process. Given that most transverse Baihetan CJB sections were quadrangular and pentagonal, we may infer that the historical basalt lava flows that formed the  $P_2\beta_3^2$  and  $P_2\beta_3^2$  strata did not follow the ideal columnar basalt formation characterized by hexagonal cross sections, most likely due to uneven or unsatisfactory temperature differences between the environment and basalt solidification temperature.

Further field studies on the jointing patterns reveal three types of joint sets that form the CJB in the diversion tunnels, as follows (Figure 4).

- Columnar joints (I): Rough surfaces that form the columnar rock block boundary. 'I' joints always intersect with each other to form columnar blocks. Their length is on a meter scale.
- Vertical internal joints (II): Found inside each columnar rock block, their plane is nearly parallel to the columnar block axes. 'II' joints are typically decimeters long and characterized by polished and wavy surfaces.
- Horizontal internal joints (III): Also found inside each columnar rock block, their plane is nearly normal to the columnar block axes; they are nearly parallel to the lava flow surface and characterized by a smooth surface, approximately 0.01–0.03 m spacing, and 0.05–0.1 m persistence.

Type 'II' and 'III' joints typically appear inside columnar jointed rock blocks in an initially closed and tight configuration before the tunnel

opening and onset of loosening due to unloading. However, they can be observed in the field due to delayed splaying after unloading excavation.

### 3.2. Micro characteristics of the joint surfaces

Scanning electron microscopy (SEM) studies have been performed to further understand the surface characteristics of the joints that form the columnar basalt rock mass structure. Several specimens were investigated using SEM, including the columnar joints and the vertical and horizontal internal joints. The SEM results indicate that each joint type has different characteristics, as follows.

- The columnar joints (I) exhibit rough surfaces on a macro scale with a micro desiccation pattern, such as a structure typical of thermal-shrinkage cracks (Figure 5a). This type of micro pattern confirms the assumption that this joint class is associated with lava cooling.
- The upright (vertical to sub-vertical in this case) internal joints (II) exhibit macroscopic smooth surfaces that are intact on the micro scale and where individual grain boundaries may be observed (Figure 5b). This micro pattern supports the assumption that upright internal joints originate from cooling-induced contraction, which may be inferred from the tensile-failed grains and wavy surfaces at the micro scale.
- The lateral (horizontal to sub-horizontal) internal joints (III) exhibit smooth surfaces on the macro scale with many parallel micro-cracks (Figure 5c). Certain shear striations were observed on the surfaces. The parallel micro-cracks might be related to the

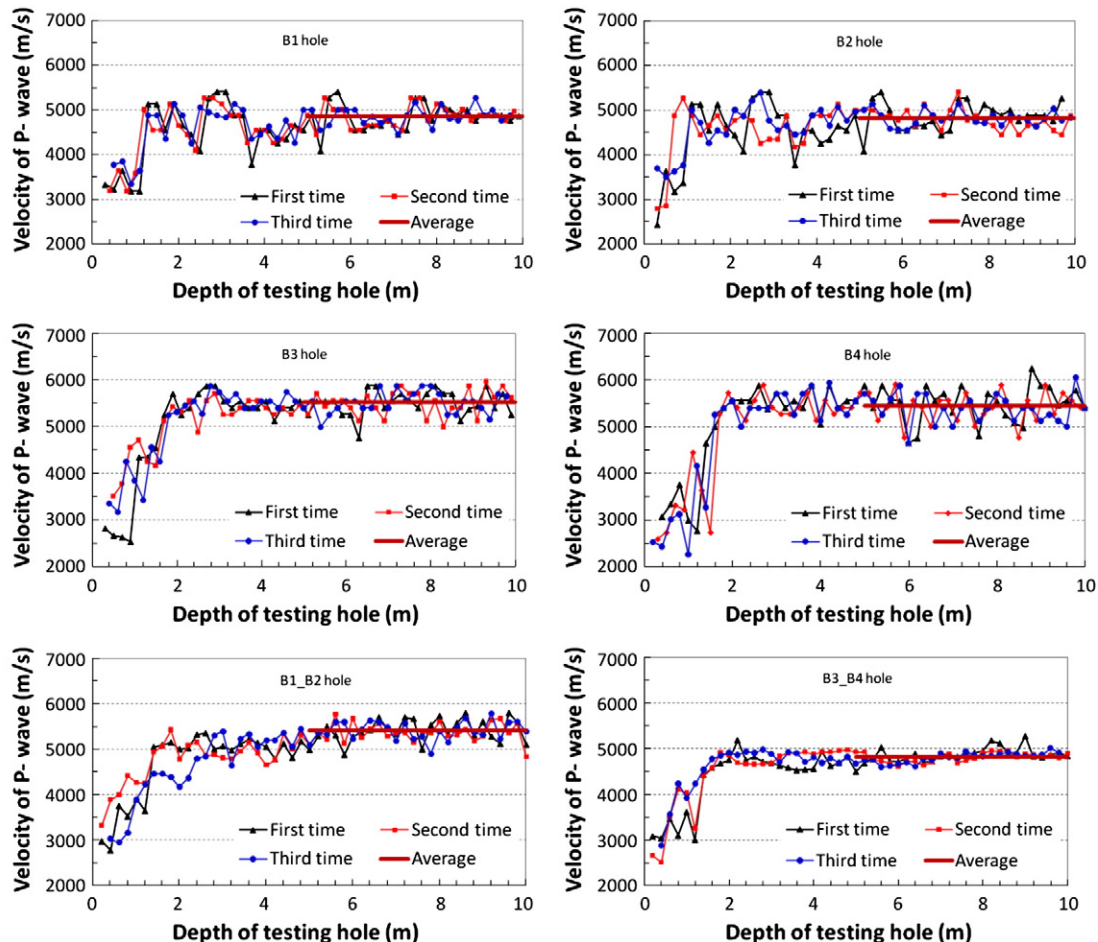


Fig. 8. The P-wave velocity profiles for boreholes B1, B2, B3 and B4 (for the location, see Figure 8).

**Table 1**  
The statistic average wave velocities of intact CJB in different transmitting directions.

Wave travel direction		Travel direction parallel to the prismatic block axis			Travel direction normal to the prismatic block axis		
		$V_{B1}$	$V_{B2}$	$V_{B3-B4}$	$V_{B3}$	$V_{B4}$	$V_{B1-B2}$
Velocity (m/s)	First time	4844	4859	4842	5539	5414	5429
	Second time	4871	4790	4814	5514	5398	5379
	Third time	4851	4803	4802	5522	5520	5417
Average P-velocity (m/s)		4830			5459		

columnar basalt crystallization process, but the frictional striations may be attributed to tectonically induced shear deformation or minute shear displacements induced by the excavation.

The two types of internal joints may also be classified as primary joints that originate from the lava cooling process. Generally, the heat exchange capability of lava layers weakens in the later cooling stages due to the appearance of multiple columnar joints (Degraff and Aydin, 1987; Saliba and Jagla, 2003; Phillips et al., 2013). As a result, the gaps between the prismatic block lateral joints become new heat-exchanging paths. Therefore, the upright internal joints that are nearly parallel to the columnar block axes may have developed due to horizontal thermal stresses. The horizontally internal joints with planes nearly perpendicular to the columnar rock block axes may also be associated with the cooling phase and later tectonic deformation. However, it is reasonable to assume that subsequent dynamic geological processes, including further volcanic and magmatic eruptions, tectonic movements, and, now engineering activities, such as blasting and excavation, also promote horizontal internal joint growth.

In sum, the CJB exhibits transverse isotropy. The isotropy plane is orthogonal to the columnar rock block axes. We identified three types of joints with different macro and micro characteristics that form the columnar jointed rock mass. The different joint sets render the rock mass a multi-scale anisotropic structure, as shown conceptually in Fig. 6. The CJB is composed of ordered prismatic blocks on the macro scale, but upright and sub-horizontal internal joints comprise the CJB structure at the micro scale. The different joint types are assumed to represent different in situ stress regimes during different time scales that are illustrated through different size scales in the rock mass. The columnar (I) joints, which are on the meter scale, control the deformation macro mechanics and dictate the shape and size of the blocks that collapse during excavation. The upright internal (II) joints, on a decimeter scale, control loosening and block collapse following unloading deformation triggered by excavation. The horizontal internal (III) joints, which are on a centimeter scale, control days-delayed rock block cracking or deformation if support was not installed in time. The CJB anisotropic characteristics studied here are clearly unique and different from other laminar or stratified anisotropic rock masses.

**4. CJB anisotropic deformability**

The field and laboratory investigation results presented above indicate that the columnar jointed basalts are inherently anisotropic, which should manifest in anisotropic mechanical behavior. In situ ultrasonic velocity tests are a rapid method for assessing CJB mechanical anisotropy (Charitaras et al., 1994; Sato et al., 2000; Kim et al., 2012; Nefeslioglu, 2013). The advantage of using *P* wave velocity tests in the field is that these experiments are not only nondestructive methods that do not require sample extraction, but they can also represent the field stress and original moisture content state of the rock mass tested. Therefore, through in situ *P* wave velocity tests, the CJB elastic deformability in different directions can be determined in the field under the existing environmental conditions.

**4.1. Testing method**

To obtain a reliable wave velocity using in situ ultrasonic velocity measurements in boreholes, the exploratory boreholes should be oriented parallel or orthogonal to the CJB transverse isotropic plane, as shown in Fig. 7a. First, the prismatic block axes orientation was measured to determine the optimum orientation of the drill holes. The resulting CJB block axis inclination was  $77^\circ/318^\circ$  (plunge/trend) at the position K0 + 550 m in the No. 2 diversion tunnel. The exploratory boreholes B1 and B2 were drilled in the tunnel floor with axes parallel to the columnar basalt axis. Both boreholes were 10 m in length and a distance of 1 m from one another. The attitude of the line between the two boreholes was designed to trend to an azimuth of  $48^\circ$ . The exploratory boreholes B3 and B4 were drilled in the sidewall; both were 10 m long with 1 m spacing between them. The B3 and B4 borehole axes were oriented normal to the columnar basalt axes ( $13^\circ/42^\circ$ ). The attitude of the line between B3 and B4 was parallel to the prismatic basalt block axes.

Ultrasonic tests were performed after drilling the exploratory boreholes (from B1 to B4). The first single borehole *P* wave velocity tests were performed in boreholes B1, B2, B3 and B4. Next, *P* wave velocity tests were performed across two boreholes for the borehole couples B1–B2 and B3–B4. As a result, we can obtain the *P*-wave velocity along

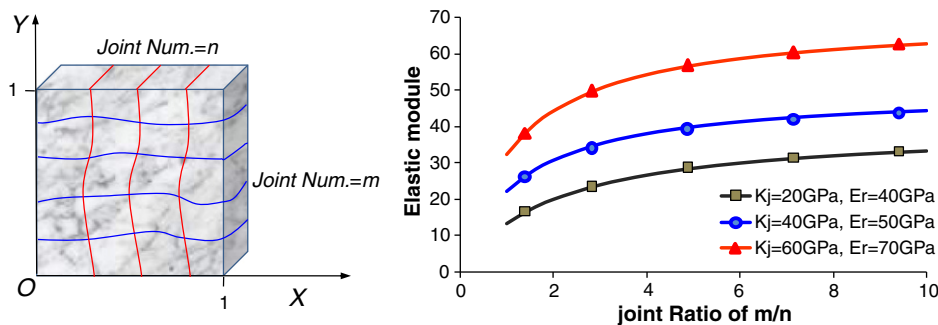


**Fig. 9.** Vertically compressive module of the joint rock mass affected by joint stiffness, the joint space ratio and the intact rock elastic moduli. The stiffness coefficient is cited from Oreste and Cravero (2008).

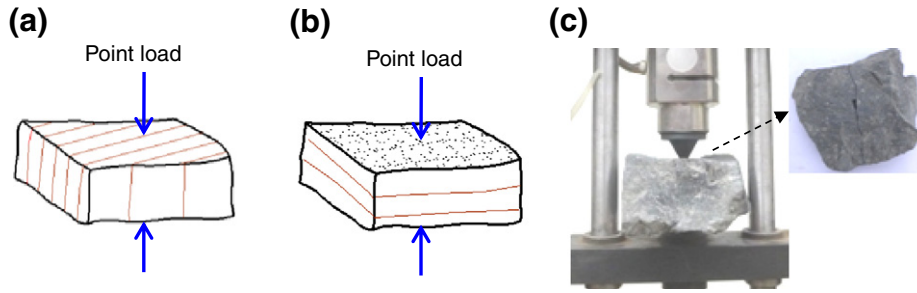


Fig. 10. Point load test configuration: (a) loading direction parallel to the transverse isotropy plane; (b) loading direction normal to the transverse isotropy plane; and (c) point load test device and representative sample used in field testing.

the transverse isotropic plane direction for the CJB using data from  $V_{B3}$ ,  $V_{B4}$  and  $V_{B1-B2}$  and the  $P$ -wave velocities along the direction normal to transverse isotropic plane using data from  $V_{B1}$ ,  $V_{B2}$  and  $V_{B3-B4}$  (Figure 7b).

#### 4.2. In situ $P$ wave velocity profiles

The above testing methodology, which was performed at position K0 + 550 m in the No. 2 diversion tunnel, provided six sets of  $P$ -wave velocity profiles for the different CJB directions. All  $P$  wave velocity profiles presented in Fig. 8 exhibit an initial low-velocity segment that was obtained in close proximity to the excavation face. These low velocity segments represent the excavation-induced damaged zone and disturbed zone with stress release, which can be determined two ways: 1) The laboratorial wave velocity of the rock core is approximately 4200 m/s on average; 2) The field image from the borehole camera showed many new surface cracks on the first 5 m borehole segment. Thus, these segments near to the free face were excluded from further analyses of the CJB intrinsic mechanical anisotropy. The representative  $P$  wave velocities for each direction were obtained by averaging the data in the linear segments of the experimentally obtained  $P$  wave velocity profiles using Eq. (1):

$$\bar{v} = \frac{1}{n} \sum_{i=1}^n v_i \quad (1)$$

where  $\bar{v}$  is the average  $P$ -wave velocity of the intact columnar jointed basalt,  $v_i$  is the measured velocity value of the  $P$ -wave on the terminal 5 m portion of the testing borehole, and  $n$  is the number of measured data. The results are reported in Table 1 for data obtained beginning 5 m from the free surface.

The average velocities, which are presented in Table 1, indicate that the average  $P$  wave velocity of an intact CJB in the direction parallel to the columnar block axes is approximately 4830 m/s, but it is approximately 5459 m/s normal to the block axis. Considering the general relationship between the dynamic moduli ( $E_d$  and  $P$  wave velocity (Eq. (2)),

the anisotropic coefficient ( $\delta$ ) obtained for the dynamic elastic modulus is 0.78 between the directions parallel and normal to the CJB axis (Eq. (3)).

$$E_d = \rho V_p^2 (1-2\nu)(1+\nu)/(1-\nu) \quad (2)$$

where,  $E_d$  is the dynamic Young's modulus of CJB,  $\rho$  is the CJB density, and  $\nu$  is the Poisson's ratio. The laboratory tests show that the dynamic Young's modulus was approximately 78.5 GPa (using the dynamic compressive test), its Poisson's ratio was approximately 0.17, and its bulk density in its natural state was approximately 2900 kg/m<sup>3</sup>.

$$\delta_d = \frac{E_{d,\parallel}}{E_{d,\perp}} = \left( \frac{V_{p,\parallel}}{V_{p,\perp}} \right)^2 \quad (3)$$

$\delta_d$  is the anisotropic coefficient of CJB's dynamic-elastic modulus;  $E_{d,\parallel}$  and  $V_{p,\parallel}$  are the dynamic Young's modulus and  $P$ -wave velocity parallel to the columnar basaltic block axis, respectively;  $E_{d,\perp}$  and  $V_{p,\perp}$  are the dynamic Young's modulus and  $P$ -wave velocity normal to the columnar basaltic block axis, respectively.

As has been previously suggested, the relationship between static and dynamic elastic moduli can typically be represented using a constant ratio (Khandelwal and Singh, 2009; Martinez et al., 2012; Nefeslioglu, 2013). Similarly, we suggest here that the relationship between the elastic constants normal and parallel to the CJB axis can be estimated using a constant, the value of which is 0.78.

It is interesting to note that the representative elastic modulus parallel to the CJB block axis is lower than that normal to the block axis. We believe that this experimental finding is related to the smaller spacing of the horizontal internal joints. Therefore, somewhat counter intuitively, waves traveling parallel to the CJB block axis are more attenuated. These results confirm Goodman's (1970) suggested relationship for estimating the elastic moduli of jointed rock masses (Eq. (4)). Inspection of Eq. (4) shows that smaller joint spacing yields a lower elastic modulus for jointed rock masses in the direction normal to the joint set plane.

$$\frac{1}{E} = \frac{1}{E_r} + \frac{1}{s \cdot K} \quad (4)$$

where,  $E$  is Young's modulus for a jointed rock mass normal to the joint planes,  $E_r$  is Young's modulus for intact rock,  $s$  is the joint spacing and  $K$  is the normal stiffness of the joints. Fig. 9 indicates that the resultant compressive modulus ( $E_v$ ) was affected by joint stiffness and elastic modulus of the intact rock to different degrees.

#### 5. Anisotropic strength of the basaltic block

The anisotropic strength of the CJB was determined using point load tests performed in the field and uniaxial compression tests performed at the laboratory.

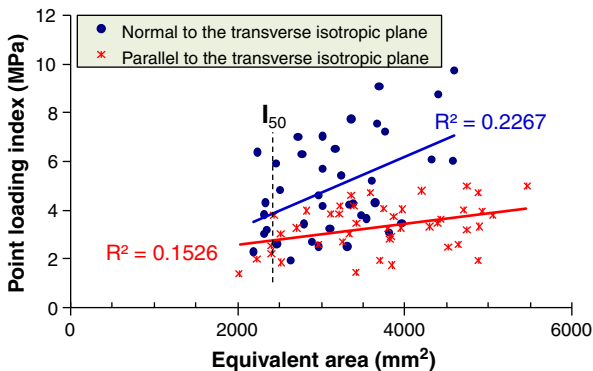


Fig. 11. Point load index of the Baihetan basalt for different size blocks.

**Table 2**

Basic mechanical parameters of the Baihetan basaltic block based on the cylinder specimens.

Source from drilling holes	Individual UCS (MPa)				Avg. UCS (MPa)	Avg. Young's moduli (GPa)	Avg. Poisson's ratio
Normal to CJB axis (B3 and B4 holes)	108.3	128.6	117.1	116.5	117.6	42.1	0.29
Parallel to CJB axis (B1 and B2 holes)	172.9	195.7	183.6	165.9	179.5	38.2	0.25

### 5.1. Point load test results

Approximately 100 basaltic block specimens were selected from the No. 4 diversion tunnel for the point load tests. Assuming that the irregular basalt blocks are anisotropic in strength, loading was applied parallel and normal to the transverse isotropic plane of the CJB (Figure 10). The tests were performed in accordance with the suggestions by the suggested method ISRM (1985) and ASTM (2002) standard. Notably, the point load values obtained from specimens retrieved at the site may reflect a certain level of damage due to blasting as well as excavation-induced rock mass relaxation.

The basaltic block point load values obtained for the loading normal and parallel to the CJB transverse isotropic plane were 39 and 44, respectively, as shown in Fig. 11. Inspection of Fig. 11 reveals that the point load strength values are somewhat scattered, and the results of these two loading configurations occasionally overlap. However, the experimental data regression analysis indicated that the size-corrected point load index ( $I_{50}^1$ ) on the anisotropic plane was approximately 3.94 MPa, and the size-corrected point load index ( $I_{50}^2$ ) on the transverse isotropic plane was approximately 2.95 MPa. Considering Broch and Franklin's (1972) suggestion and the report from the IRSM Commission on Standardization of Laboratory and Field Tests (ISRM, 1985), the multiplying factor between the UCS and point load strength can be '24' for hard, strong rocks. Thus, the equivalent uniaxial compressive strength (UCS) for Baihetan's CJB normal and parallel to the representative block axis may be estimated at 71 MPa and 95 MPa, respectively. Clearly, the anisotropic signature is evident. In general, quantitatively, the

anisotropic coefficient for compressive strength ( $\delta_s$ ) is estimated at approximately 0.75 using Eq. (5) (ASTM, 2002).

$$\delta_s = I_{50}^2 / I_{50}^1 \quad (5)$$

### 5.2. Uniaxial compression tests

Solid cylinders 50 mm in diameter and 100 mm long that were retrieved from experimental boreholes B1 to B4 were prepared for uniaxial compression tests following the ISRM suggested method standards (Fairhurst and Hudson, 1999). Cylinders were prepared with axes normal and parallel to the CJB block axis, respectively. Laboratory test results indicate that the average UCS for basalt cylinders with axes parallel to the transverse isotropic plane (normal to the CJB block axis) was approximately 117.6 MPa, whereas the average UCS of basalt cylinders with axes normal to the transversely isotropic plane (parallel to the CJB block axis) was approximately 179.5 MPa (Table 2 and Figure 12). The test results also indicate that the average Young's modulus for the basalt specimens with axes normal and parallel to the CJB block axis are 42.1 GPa and 38.2 GPa, respectively; their average Poisson ratios are 0.29 and 0.25, respectively (seeing Table 2). The ratio between the two representative UCS values was approximately 0.67. Interestingly, the anisotropic coefficients obtained using the different testing methods all appear similar considering that the blasting could have caused some damage to the basalt blocks used for the point load tests.

## 6. Discussion

Many rock mass classification systems have been proposed and used to estimate stability and support geotechnical engineering design, such as the RQD (Deere, 1968), rock mass rating (Bieniawski, 1976), Q index (Barton et al., 1974), GSI index (Hoek et al., 1998) and Rmi system (Palmstrom, 1996). However, determining the generalized mechanical parameters for the jointed rock mass remains one of the most difficult and challenging tasks in rock engineering. Among the proposed classification methods, the GSI index with the corresponding RocLab software (Rocscience Inc., 2007) provided an adequate approach for estimating mechanic parameters of columnar jointed basalt rock masses. This approach can provide a set of quantitative mechanical properties (such as deformational model and tensile strength) for numerical analyses and reinforcement designs because it does not ignore key factors, such as rock structure, block surface and excavation quality (Hoek and Brown, 1997; Cai et al., 2004). Indeed, there have been many attempts to extend the GSI method to apply to anisotropic rock masses (Wu and Wang, 2001; Hoek and Marinos, 2005; Budetta and Nappi, 2011; Fortsakis et al., 2012).

Using the results reported here, we attempt to estimate the mechanical properties of the CJB rock mass studied using the GSI index. Because the joint distribution in the isotropy plane may be assumed homogeneous (Hoek and Brown, 1997; Cai et al., 2004), we consider the basaltic rock mass equivalent to an H–B rock mass on its transversely isotropic plane; as a result, its mechanical parameters can be estimated using the GSI index (see Figure 6). Next, the basic deformational and strength parameters can be inferred from the CJB anisotropic coefficients obtained. To estimate the CJB parameters on the transverse isotropy plane, several input parameters for the RocLab software were determined,

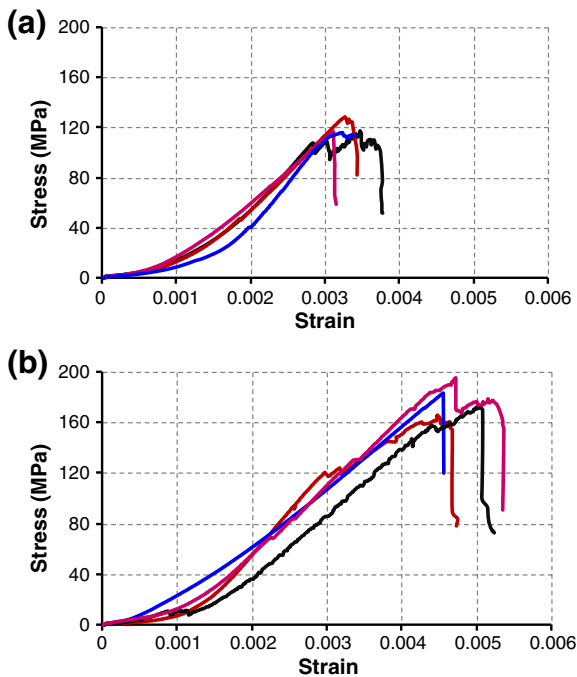


**Fig. 12.** Typical axial stress–strain curves of different basalt specimens (a. loading direction parallel to the transversely isotropic plane; and b. loading direction normal to the transversely isotropic plane).

**Table 3**  
Input parameters for RocLab to estimate the mechanical parameters for the CJB transverse isotropy plane.

UCS of the intact rock (MPa)	GSI	$M_i$	$D$	$E_i$ of the intact rock (GPa)	Application	Density ( $\text{kg/m}^3$ )	Depth (m)
117.6	60	20	0.2	42	Tunnel	2900	400

**Table 4**  
Estimated mechanical parameters for the CJB based on the RocLab software.

Parameters of rock mass	Deformational module (GPa)	Global strength (MPa)	Tensile strength (MPa)	$m_b$	$s$
On the transverse isotropic plane	17.2	32.4	0.25	4.1	0.0085
On the anisotropic plane	13.4	45.6	0.35	5.8	0.012

Note: The anisotropy coefficient of deformability was 0.78, the anisotropy coefficient of strength was 0.71, and the  $m_b$  and  $s$  were Hoek–Brown criterion constants.

considering the field investigation and experimental tests (as Table 3). As a result, estimated mechanical parameters for the CJB on the transverse isotropic plane were obtained using RocLab software, and the mechanical parameters for the CJB anisotropic plane were also estimated based using the anisotropic coefficient obtained (as Table 4). Certain field monitoring data have partially verified the reasonability of the estimated mechanical parameters. For example, the displacement measured using a multi-point meter showed that the unloading deformation on the tunnel roof was greater than that on the tunnel sidewall (Figure 13), which is consistent with the estimated parameters showing that the CJB deformation module on the anisotropic plane was smaller than on the transverse isotropic plane (seeing Table 4). With these key anisotropic parameters for the CJB, further numerical simulations are possible for reliable stability evaluations and optimal designs for underground tunnels or caverns in columnar jointed basalt rock masses.

## 7. Summary and conclusions

Our field investigations indicate that most transverse sections of the Baihetan's columnar jointed basalt block were not hexagonal, but quadrangular or pentagonal, and their edge lengths were typically in the range 0.12 to 0.24 m. The interface morphology for the three types of joint sets that formed the Baihetan's columnar jointed basalt mass were also studied using SEM observations. These results with different surface characteristics provide insight into the Baihetan's columnar jointed basalt mass formation mechanism.

The columnar joint sets and other internal joint sets played a crucial role in determining the mechanical properties of the Baihetan's columnar jointed basalt and generated its transverse isotropy plane normal to

the columnar basalt block axes. This plane yields higher  $P$  wave velocity values when the wave propagation path is normal to the CJB block axis and higher unconfined compression strengths when the tested cylinders are aligned parallel to the CJB block axis. The same result was obtained from point load testing. We show that the lower  $P$  wave velocity parallel to the CJB block axis was caused by the closely spaced transverse sub-horizontal planes. However, their presence does not seem to affect the compressive strength, which appears higher when compression is applied in a direction parallel to the CJB block axis, which is primarily normal to the closely spaced sub-horizontal joints.

An interesting and important result is that the mechanical deformability and strength anisotropic coefficients for the Baihetan's columnar jointed basalt mass are relatively similar for all testing methods employed, including the in situ  $P$  wave velocity, point load, and uniaxial compression tests. This result confirms the strong anisotropic effect in these rock masses and facilitates the relevant assessment of mechanical parameters as input parameters in rock mass classification schemes or numerical simulation estimation.

The mechanical parameters and constants for the Hoek–Brown criterion mechanical parameters and constants were also tentatively obtained based on the GSI index and corresponding RocLab software utilizing the experimentally obtained anisotropic coefficients. With these key CJB mechanical parameters, a more reliable numerical prediction is possible for mechanical response and stability analysis for columnar jointed basalts during underground excavations.

## Acknowledgments

The authors gratefully acknowledge the financial support from National Natural Science Foundation of China (Grant No. 41172284 and No. 51379202). Y. Hatzor wishes to thank the Chinese Academy of Sciences for a visiting professorship grant awarded to senior international scientists (No. 2011T2G29). In particular, authors also wish to thank Prof. Y.L. Fan, Prof. X.D. Zhu and Prof. A.C. Shi for their kind help in the field investigation and the technical support from China Three Gorges Project Corporation.

## References

- ASTM, 2002. Standard test method for determination of the point load strength index of rock. Current Edition Approved Nov. Annual Book of ASTM Standards, West Conshohocken, United States, Vol. 04.08 (D5731-02).
- Barton, N., Bandis, S., 1980. Some effects of scale on the shear strength of joints. *Int. J. Numer. Anal. Met.* 17, 69–73.
- Barton, N.R., Lien, R., Lunde, J., 1974. Engineering classification of rock masses for the design of tunnel support. *Rock Mech.* 6 (4), 189–239.
- Bieniawski, Z.T., 1976. Rock mass classification in rock engineering. In: Bieniawski, Z.T. (Ed.), *Exploration for Rock Engineering*, Proceedings of the Symposium, Vol. 1. Balkema, Rotterdam, pp. 97–106.
- Brady, B.H.G., Brown, E.T., 1985. *Rock Mechanics for Underground Mining*. Springer, P.O. Box 17,3300 AA Dordrecht, The Netherlands.
- Broch, E., Franklin, J., 1972. The point-load strength test. *Int. J. Rock Mech. Min. Sci. Geomech. Abstr.* 9 (6), 669–676.

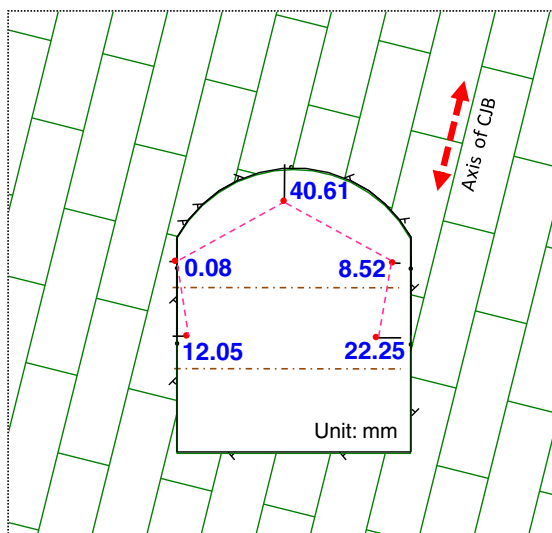


**Fig. 13.** In-situ measured displacement of columnar jointed basalt mass at the diversion tunnel (No. 4, K1 + 075) during the tunnel opening layer by layer.

- Budetta, P., Nappi, M., 2011. Heterogeneous rock mass classification by means of geological strength index: the San Mauro formation (Cilento, Italy). *Bull. Eng. Geol. Environ.* 70 (4), 585–593.
- Budkewitsch, P., Robin, P.Y., 1994. Modelling the evolution of columnar joints. *J. Volcanol. Geotherm. Res.* 59, 219–239.
- Cai, M., Kaiser, P.K., Uno, H., Tasaka, Y., Minami, M., 2004. Estimation of rock mass deformation modulus and strength of jointed hard rock masses using the GSI system. *Int. J. Rock Mech. Min. Sci.* 48 (41), 3–19.
- Christaras, B., Auger, F., Mosse, E., 1994. Determination of the moduli of elasticity of rocks: comparison of the ultrasonic velocity and mechanical resonance frequency methods with direct static methods. *Mater. Struct.* 27, 222–228.
- Cundall, P.A., Fairhurst, C., 1987. Correlation of numerical and physical models – an approach to the estimation of rock mass behaviour. *Comput. Geotech.* 3 (1), 62.
- Deere, D.U., 1968. Geological consideration. In: Stagg, K.G., Zienkiewicz, O.C. (Eds.), *Rock Mechanics in Engineering Practice*. Wiley, New York.
- Degraff, J.M., Aydin, A., 1987. Surface morphology of columnar joints and its significance to mechanics and direction of joint growth. *Geol. Soc. Am. Bull.* 99 (5), 605–617.
- Degraff, J.M., Long, P.E., Aydin, A., 1989. Use of joint-growth directions and rock textures to infer thermal regimes during solidification of basaltic lava flows. *J. Volcanol. Geotherm. Res.* 38, 309–324.
- Diego, M.I., Matthew, E.P., Caroline, D., et al., 2011. The synthetic rock mass approach for jointed rock mass modelling. *Int. J. Rock Mech. Min. Sci.* 48, 219–244.
- Fairhurst, C.E., Hudson, J.A., 1999. Draft ISRM suggested method for the complete stress-strain curve for intact rock in uniaxial compression. *Int. J. Rock Mech. Min. Sci.* 36, 279–289.
- Fang, S., Li, J., Wu, S., et al., 2011. Large six-party columnar joints of acidic volcanic rocks and its geological causes and significance in Hong Kong China. *Mar. Sci.* 35 (5), 89–94 (in Chinese).
- Fortsakis, P., Nikas, K., Marinos, V., Marinos, P., 2012. Anisotropic behaviour of stratified rock masses in tunnelling. *Eng. Geol.* 141–142, 74–83.
- Fuenkajorn, K., Phueakphum, D., 2010. Physical model simulation of shallow openings in jointed rock mass under static and cyclic loadings. *Eng. Geol.* 113, 81–89.
- Gadde, M., Rusnak, J., Honse, J., et al., 2007. On rock failure criteria for coal measure rocks. 26th International Conference on Ground Control in Mining, Morgantown, USA, pp. 361–369.
- Genger, M., 1985. Progressive failure in stratified and jointed rock mass. *Rock Mech. Rock. Eng.* 18, 267–292.
- Goehring, L., Morris, S.W., 2008. Scaling of columnar joints in basalt. *J. Geophys. Res.* 113 (B10), 1–18.
- Goehring, L., Lin, Z., Morris, S.W., 2006. An experimental investigation of the scaling of columnar joints. *Phys. Rev. E* 74 (036115), 1–13.
- Goodman, R.E., 1970. *Introduction to Rock Mechanics*. John Wiley and Sons, New York p. 478.
- Hetenyi, G., Taisne, B., Fanny, Garel, et al., 2012. Scales of columnar jointing in igneous rocks: field measurements and controlling factors. *Bull. Volcanol.* 74, 457–482.
- Hoek, E., Brown, E.T., 1980. Empirical strength criterion for rock masses. *J. Geotech. Eng. Div. ASCE* 106 (9), 1013–1035.
- Hoek, E., Brown, E.T., 1997. Practical estimates of rock mass strength. *Int. J. Rock Mech. Min. Sci.* 48, 34 (8), 1165–1186.
- Hoek, E., Marinos, P.G., 2005. Characterization and engineering properties of tectonically undisturbed but litho logically varied sedimentary rock masses. *Int. J. Rock Mech. Min. Sci.* 42, 277–285.
- Hoek, E., Marinos, P., Benissi, M., 1998. Applicability of the geological strength index (GSI) classification for very weak and sheared rock masses: the case of Athens Schist Formation. *Bull. Eng. Geol. Environ.* 57, 151–160.
- Hudson, J.A., Priest, S.D., 1983. Discontinuity frequency in rock masses. *Int. J. Rock Mech. Min. Sci. Geomech. Abstr.* 20 (2), 73–89.
- Ibarra, J.A., Maerz, N.H., Franklino, J.A., 1996. Overbreak and underbreak in underground openings part 2: causes and implications. *Geotech. Geol. Eng.* 1996 (14), 325–340.
- Ishida, T., Uchita, Y., 2000. Strain monitoring of borehole diameter changes in heterogeneous jointed wall rock with chamber excavation; estimation of stress redistribution. *Eng. Geol.* 56, 63–74.
- ISRM, 1985. International Society for Rock Mechanics Commission on testing methods: suggested methods for determining point load strength. *Int. J. Rock Mech. Min. Sci. Geomech. Abstr.* 22 (2), 51–60.
- Jaeger, J.C., Cook, N.G.W., Zimmerman, R.W., 2007. *Fundamentals of Rock Mechanics*. Blackwell Publishing, Fourth, MA.
- Jia, P., Tang, C.A., 2008. Numerical study on failure mechanism of tunnel in jointed rock mass. *Tunn. Undergr. Space Technol.* 23, 500–507.
- Khandelwal, M., Singh, T.N., 2009. Correlating static properties of coal measure rocks with P-wave velocity. *Int. J. Coal Geol.* 79, 55–60.
- Kim, H., Cho, J.W., Song, I., Min, K.B., 2012. Anisotropy of elastic moduli, P-wave velocities, and thermal conductivities of Asan Gneiss, Boryeong Shale, and Yeoncheon Schist in Korea. *Eng. Geol.* 147–148, 68–77.
- Lore, J., Gao, H., Aydin, A., 2000. Viscoelastic thermal stress in cooling basalt flows. *J. Geophys. Res.* 105, 23695–23709.
- Maghous, S., Bernaud, D., Freard, J., Garnier, D., 2008. Elastoplastic behavior of jointed rock masses as homogenized media and finite element analysis. *Int. J. Rock Mech. Min. Sci.* 45, 1273–1286.
- Mahendra, S., Bhawani, S., 2008. High lateral strain ratio in jointed rock masses. *Eng. Geol.* 98, 75–85.
- Martinez, J.M., Benavente, D., Garca-del-Cura, M.A., 2012. Comparison of the static and dynamic elastic modulus in carbonate rocks. *Bull. Eng. Geol. Environ.* 71, 263–268.
- Moon, V., Bradshaw, J., Smith, R., Lange, W., 2005. Geotechnical characterization of stratocone crater wall sequences, White Island Volcano, New Zealand. *Eng. Geol.* 81, 146–178.
- Müller, G., 1998. Starch columns: analog model for basalt columns. *J. Geophys. Res.* 103, 15239–15253.
- Nefeslioglu, H.A., 2013. Evaluation of geo-mechanical properties of very weak and weak rock materials by using non-destructive techniques: ultrasonic pulse velocity measurements and reflectance spectroscopy. *Eng. Geol.* 160, 8–20.
- Oreste, P.P., Craverio, M., 2008. An analysis of the action of dowels on the stabilization of rock blocks on underground excavation walls. *Rock Mech. Rock. Eng.* 41, 835–868.
- Palmstrom, A., 1996. Characterizing rock masses by the RMI for use in practical rock engineering, part 1: the development of the rockmass index (RMI). *Tunn. Undergr. Space Technol.* 11 (2), 175–188.
- Pariseau, W.G., 1999. An equivalent plasticity theory for jointed rock masses. *Int. J. Rock Mech. Min. Sci.* 36, 907–918.
- Peck, D.L., Minakami, T., 1968. The formation of columnar joints in the upper part of Kilauean lava lakes. *Geol. Soc. Am. Bull.* 79, 1151–1166.
- Phillips, J.C., Humphreys, M.C.S., Daniels, K.A., Brown, R.J., 2013. The formation of columnar joints produced by cooling in basalt at Staffa, Scotland. *Bull. Volcanol.* 75 ((7), 715), 1–18.
- Rocscience Inc., 2007. Rock mass strength analysis using the generalized Hoek–Brown failure criterion (RockLab, V1.031). <http://www.rocscience.com/products/14>.
- Saliba, R., Jagla, E.A., 2003. Analysis of columnar joint patterns from three-dimensional stress modeling. *J. Geophys. Res.* 108 (B10), 1–7.
- Sato, T., Kikuchi, T., Sugihara, K., 2000. In-situ experiments on an excavation disturbed zone induced by mechanical excavation in Neogene sedimentary rock at Tono mine, central Japan. *Eng. Geol.* 56, 97–108.
- Shi, A.C., Tang, M.F., Shan, Z.G., 2006. Feasibility Report of Baihetan Hydropower Station in Jinsha river: Geological Investigation of Columnar Jointed Rock Mass. East China Investigation and Design Institute, China Hydropower Electric Consultant Corporation, Hangzhou (in Chinese).
- Shi, A.C., Tang, M.F., Zhou, Q., 2008. Research of deformation characteristics of columnar jointed basalt at Baihetan hydropower station on Jinsha river. *Chin. J. Rock Mech. Eng.* 27 (10), 2079–2086 (in Chinese).
- Sousa, L.R., 2006. Learning with accidents and damage associated with underground works. In: Matos, C., Sousa, R., Pinto, L. (Eds.), *Geotechnical Risks in Rock Tunnels*. Taylor & Francis, London, pp. 7–39.
- Waltham, A.C., Swift, G.M., 2004. Bearing capacity of rock over mined cavities in Nottingham. *Eng. Geol.* 75, 15–31.
- Wang, S.L., Yin, S., Wu, Z., 2011. Strain-softening analysis of a spherical cavity. *Int. J. Numer. Anal. Met.* 36 (2), 182–202.
- Wu, F.Q., Wang, S.J., 2001. A stress-strain relation for jointed rock masses. *Int. J. Rock Mech. Min. Sci.* 591–598.
- Xu, W.Y., Deng, W.T., Ning, Y., et al., 2010. 3D anisotropic numerical analysis of rock mass with columnar joints for dam foundation. *Rock Soil Mech.* 31 (3), 949–955 (in Chinese).
- Xu, J.J., Xu, J.R., He, M.J., 2011. Study on the shape of Baihetan nonsymmetrical arch dam. *Water Power* 37 (3), 32–35 (in Chinese).
- Yan, D.X., Xu, W.Y., Zheng, W.T., et al., 2011. Mechanical characteristics of columnar jointed rock at dam base of Baihetan hydropower station. *J. Cent. South Univ.* 18, 2157–2162.
- Yoshida, H., Horii, H., 2004. Micromechanics-based continuum model for a jointed rock mass and excavation analyses of a large-scale cavern. *Int. J. Rock Mech. Min. Sci.* 41, 119–145.
- Zhang, H., Zhu, J., Liu, Y., et al., 2012. Strength properties of jointed rock masses based on the homogenization method. *Acta Mech. Solida Sin.* 25 (2), 177–185.
- Zhu, B.Q., Mao, C.X., Lugmair, G.W., et al., 1985. Isotopic and geochemical evidence for the origin of Plio–Pleistocene volcanic rocks near the Indo–Eurasian collisional margin at Tengchong, China. *Earth Planet. Sci. Lett.* 65 (2), 263–275.